Exploration of the physical states of riboflavin (free base) by mechanical milling

Charline Henaff, Juergen Siepmann, Florence Siepmann, Florence Danede, Marie-Noëlle Avettand-Fènoël, Jérémy Verin, Alexandre Fadel, Jean-François Willart

Exploration of the physical states of riboflavin (free base) by mechanical milling

C. Henaff[1,2], J. Siepmann[2], F. Siepmann[2], F. Danède[1], M.-N. Avettand-Fènoël[1], J. Vérin[2], A. Fadel[3], J.-F. Willart[1]

[1] Univ. Lille, CNRS, INRAE, Centrale Lille, UMR 8207
UMET - Unité Matériaux et Transformations F-59000 Lille, France

[2] Univ. Lille, Inserm, CHU Lille, U1008, F-59000 Lille, France

[3]Univ. Lille, CNRS, INRAE, Centrale Lille, Univ. Artois, FR 2638 - IMEC - Institut Michel-Eugène Chevreul, F-59000 Lille, France

Corresponding author: Jean-François Willart

Abstract

Amorphous riboflavin (free base) could be produced for the first time via high energy ball milling of a commercial crystalline form (Form I). Importantly, this solid state amorphization process allowed to circumvent chemical degradation occurring during melting as well as the lack of suitable solvents, which are required for amorphization via spray- or freeze-drying. The amorphous state of riboflavin was thoroughly characterized, revealing a complex recrystallization pattern upon heating, involving two enantiotropic polymorphic forms (II and III) and a dihydrate. The glass transition temperature (Tg) and heat capacity (Cp) jump of the amorphous form were determined as 144°C and 0.68 J/g/°C. Moreover, the relative physical stability of the different physical states has been elucidated, e.g., at room temperature: I > II > III. The following rank order was observed for the dissolution rates in water at 37 °C during the first 4 h: amorphous > III ≈ II> I. Afterwards, a dihydrate crystallized from the solutions of amorphous and metastable crystalline riboflavin forms, the solubility of which was well above the solubility of the stable Form I.

1. Introduction

Drugs can exist in different physical states, like stable and metastable polymorphic forms [1]–[4], or in an amorphous form [5], [6]. These different forms can potentially have a strong repercussion on their key properties, including in particular their stability during storage [7], [8] and their solubility in aqueous body fluids [9], [10]. Thus, the physical state of a drug might substantially impact the therapeutic efficacy of the treatment. In general, the solubility of a drug increases when the Gibbs free energy of the physical form increases. Thus, often an improvement in solubility comes at the expense of physical stability [11], [12]. Controlling and manipulating the physical state of drugs is, hence, an important practical challenge, in particular for the formulation of poorly soluble drugs [13]–[16]. Furthermore, the physical state of a drug might change during manufacturing and long-term storage [17]. This is why it is essential to explore as thoroughly as possible all the physical states of a drug, their physical (and chemical) (in)stabilities, as well as their solubility and dissolution kinetics [18], [19].

Several processes can be used to render a drug amorphous, including melt quenching [20], hot melt extrusion [21], [22],[23], spray-drying [24], [25], freeze-drying [26], [27], high shear granulation [28] and mechanical milling [29]. The technology “KinetiSol® Dispersing” combines the effects of fusion/heat and frictional/shear energies [30]. Melt quenching and hot melt extrusion have the disadvantage of the need to heat the material up to its melting point, which often induces unacceptable thermal degradation. Spray-drying and freeze-drying require the dissolution of the drug in a solvent, which can also induce chemical changes like mutarotation [31]. Moreover, finding an effective and non-toxic solvent is often a challenge for poorly soluble drugs. Contrary to the previous techniques, the amorphization upon *milling* occurs directly in the solid state, so that it does not require any heating or dissolution stages of the drug. Milling, thus, often allows rendering drugs amorphous without any chemical changes, so that it appears as an interesting alternative to the other amorphization techniques.

Riboflavin ($C_{17}H_{20}N_4O_6$) free base, also known as vitamin B2, is a coenzyme in oxidation and reduction reactions [32]. It is essential for cell growth, and commonly used in parenteral nutrition [33]. Even if it is considered to be a “water soluble” vitamin [34], its solubility in this solvent is very limited, as it only reaches around 0.08 mg/mL at 30°C [35]. Evidence of polymorphism was briefly mentioned in the literature along with different hydrates [36], [37]. However so far, to the best of our knowledge, only the crystalline structure of the commercial form (Form I) could be determined and was found to be orthorhombic (space group $P2_12_12_1$) [38]. Moreover, little is known about its amorphous state, which cannot be obtained by quenching the liquid (because of a pronounced chemical degradation upon melting), nor by spray- or freeze-drying due to the lack of an appropriate solvent [35], [39].

The objective of this paper was to use high energy milling to prepare and thoroughly characterize the amorphous state of riboflavin (free base), which is currently poorly investigated (including for instance the determination of its glass transition temperature and the related heat capacity jump). Special attention was paid to the recrystallization mechanism of the amorphous form upon heating, which revealed to be complex, involving two polymorphic forms. Moreover, the relative stability of the different physical states of riboflavin were to be established and their dissolution kinetics in water at 37 °C to be monitored.

2. Materials and Methods

2.1. Materials

Riboflavin free base (purity 98%), also known as vitamin B2, was purchased from ACROS organics (Geel, Belgium). The material was used as received. Ultra-pure water was obtained from Veolia (Vendin le Vieil, France), acetonitrile (HPLC grade) from Carlo Erba (Val de Reuil, France), formic acid and dimethyl sulfoxide from Sigma Aldrich (Seelze, Germany).

2.2. Ball milling

Ball milling was performed at room temperature (RT) using a high energy planetary mill (Pulverisette 7 Fritsch, Idar Oberstein, Germany). About 1.1g samples were placed into ZrO_2 milling vessels (40mL), containing 7 milling balls (ZrO_2, Ø = 15mm) in order to have a ball/sample ratio of 75:1 w/w. The rotation speed of the solar disk was set to 400 rpm. The reverse mode was selected, so that after each milling cycle, the direction of rotation changed. This rotation speed corresponded to an average acceleration of the milling balls of 5 g (g = 9.81 m/s^2 being the acceleration of gravity). Milling cycles (20 min) were alternated with pause periods (10 min) in order to prevent heating of the samples during the process. Heat-sensitive stickers on the milling vessels indicated that the temperature of the latter reached approximately 35°C under the given conditions [40]. The milling times (t_m) were varied between “zero” (non-milled material) and 32 h, as indicated.

2.3. Thermogravimetric analysis (TGA)

TGA measurements were performed using the Q500 apparatus from TA instruments (Guyancourt, France). A small amount of sample (between 5 and 8 mg) was placed into an open aluminum pan on a weighing scale. Both, the sample and the weighing scale, were kept in a dry atmosphere using a constant flow rate (50 mL / min) of highly pure nitrogen gas (99.999 %). The temperature reading was calibrated with the

measurements of the Curie points of alumel and of nickel (provided by TA instruments). The mass reading was calibrated using certified calibration weights (TA instruments). All scans were performed at 5 °C/min from room temperature to 550 °C.

2.4. Differential Scanning Calorimetry (DSC)

DSC thermograms were recorded with a Q20 apparatus from TA Instruments (Guyancourt, France), connected to a refrigerated cooling system. During all measurements, the calorimeter head was flushed (50 mL/min) with highly pure nitrogen gas (99.999 %). Temperature and enthalpy readings were calibrated using pure indium at the same scan rates as used during the measurements. Small sample sizes (between 2 and 5 mg) were used to provide good thermal conductivity and sharp enthalpic events. The samples were placed in open aluminum pans (container without lid) to allow the release of free water, potentially adsorbed during the milling process. Only when heating to temperatures above the degradation temperature of riboflavin, hermetic high-pressure aluminum pans were used (to avoid any contamination of the DSC cell). For all samples, a preliminary 20 min annealing at 90°C was performed in the DSC in order to remove, as much as possible, the water absorbed during the sample preparation. All scans were performed using an average heating rate of 5 °C/min.

2.5. Hyper Differential Scanning Calorimetry (Hyper DSC)

Hyper DSC scans were recorded at a heating rate of 300 °C/s using the Flash DSC2+ from Mettler Toledo (Viroflay, France), under argon flushing. The high scanning rate allowed by-passing transformations which are kinetically slow, like recrystallizations or polymorphic transformations.

2.6. Powder X-Ray Diffraction (PXRD)

Powder X-ray diffraction measurements were performed with a PanAlytical X'PERT PRO MPD (Almelo, The Netherlands) diffractometer (λCuK_α = 1.5418 Å for combined

$K_\alpha 1$ and $K_\alpha 2$), equipped with an X'celerator detector (Almelo, The Netherlands) allowing acquisition of diffraction patterns from 2θ= 3 to 60 °, with a scan step of 0.0167 °/s. Samples were placed into Lindemann glass capillaries (Ø = 0.7 mm), installed on a rotating sample holder to avoid artifacts due to preferential orientations of crystallites. Thermal treatment of the samples was performed in the calorimeter, followed by sample removal from the DSC pan and immediate PXRD analysis. In some specific cases, to observe the evolution of the sample upon heating, the sample was placed on a metallic plate, in an Anton Paar chamber at atmospheric pressure. The heating rate was set to 5 °C/min.

2.7. ^{1}H Nuclear Magnetic Resonance (NMR)

NMR analyses were conducted on a Brucker AVANCE 300 MHz apparatus (Rheinstetten, Germany) at 20°C. A few milligrams of material were dissolved in 0.5 mL dimethyl sulfoxide in 5 mm diameter NMR tubes. For each sample, 64 scans were recorded (1 scan/s) to improve the signal statistic.

2.8. Scanning electron microscopy (SEM)

SEM pictures were taken to determine the morphology of the particles, using a JEOL Field Emission apparatus (JSM-7800F, Tokyo, Japan). Samples were mounted on a SEM stub, using ribbon carbon double-sided adhesive. To avoid surface charging, samples were chromium coated (100 Å) by electro-sputting under vacuum prior to SEM observations. The observations were performed at 2 kV acceleration voltage, with small probe current and the lowest objective lens aperture to reduce beam damage on the sample surface.

2.9. Riboflavin dissolution kinetics

Excess amounts of riboflavin (about 150 mg) were exposed to 10 mL ultra-pure water in amber flasks. The latter were placed into a horizontal shaker (37 °C, 80 rpm; GFL 3033; Gesellschaft fuer Labortechnik, Burgwedel, Germany). At predetermined time

points, 300 µL samples were withdrawn, filtered (PVDF syringe filter 0.22 µm, Agilent technologies, Santa Clara, USA) and analyzed for their riboflavin content by reverse phase HPLC-UV analysis (Waters Alliance 2695 separation module, Waters 2489 UV/vis detector) as follows: 10 µL samples were injected into a polar column (Luna omega 3 µm C18 100 Å, 150 x 4.6 mm; Phenomenex, Le Pecq, France). The flow rate was set to 0.8 mL/min. The mobile phase was a 85:15 (v:v) blend of 0.1% aqueous formic acid solution and acetonitrile. The column was kept at room temperature and the detection wavelength was set to 270 nm. The calibration curve was determined for riboflavin concentrations ranging from 0.1 to 40 mg/L ($R^2 > 0.999$). Each experiment was performed in triplicate. Mean values +/- standard deviations are reported.

3. Results and Discussion

3.1. Solid state amorphization by milling

The blue curve at the top of Figure 1 shows the X-ray diffraction patterns of commercial riboflavin (used as received) recorded at room temperature. It shows many Bragg peaks, which are characteristic of a crystalline state and their positions correspond to that of Form I, recently determined by Guerain et al. [38]. The black curve in Figure 2 shows the TGA scan of a commercial riboflavin (Form I), recorded upon heating (5 °C/min). It shows a significant weight loss (about 70%) starting above 250 °C, revealing a pronounced thermal degradation of the vitamin. Figure 2 also shows the heating DSC scan (5 °C/min) of riboflavin placed in a hermetically closed, high-pressure pan (run 1). It reveals a sharp endothermic peak around 290 °C, which superimposes on a wide exothermic event. The endotherm corresponds to the melting of Form I, while the exotherm is due to the chemical degradation revealed by TGA (Figure 2). It is worth noting that degradation starts slightly before melting, indicating that the degradation is not due to the melting process itself. This degradation was already reported in literature [41] and prevents from accurately determining the melting

temperature of the vitamin and from safely obtaining the amorphous form via a classical quench of the liquid. Figure 3 shows the ^{1}H NMR spectra of both, crystalline (Form I) and melted riboflavin, after dissolution in dimethyl sulfoxide. The two spectra show significant differences, as many new peaks appeared after the melting (e.g. between 2.0 and 2.3 ppm, between 3.8 to 4.2 ppm, between 7.1 to 7.8 ppm and at 11.3 ppm). These peaks confirm the chemical degradation of riboflavin upon melting and the impossibility to obtain the amorphous state by quenching the melt. To overcome this hurdle, we tried to obtain the amorphous state directly in the solid state, by milling [42] the crystalline Form I.

The red curve in Figure 1 shows the X-ray diffraction patterns of riboflavin Form I after 32 h milling. It can be noticed that all Bragg peaks have completely disappeared, leading to the appearance of a large halo of diffusion, characteristic for an amorphous form. The red curve in Figure 2 shows the corresponding heating DSC scans (5 °C/min): recorded using an open pan from 45 to 240 °C (run 2) and a hermetically closed, high pressure pan from 240 to 310 °C (run 3). This latter type of pan was used to avoid the contamination of the DSC cell by the degradation products generated upon melting. The 2 vertical slashes separate the two runs. Run 2 shows a heat capacity (Cp) jump (ΔCp = 0.68 J/g/°C), characteristic of a glass transition. This proves that a direct “crystal to glass transformation” occurred during the milling process. The red curve in Figure 3 shows the ^{1}H NMR spectrum of amorphous riboflavin obtained by milling Form I (32 h). It appears to be identical with the spectrum of the commercial riboflavin, except for one peak at 2.09 ppm, which is attributed to an acetone residue [43], stemming from the cleaning of the NMR tube. Moreover, no signs of chemical degradation were detected compared to the spectrum of the quenched liquid. It, thus, appears that mechanical milling is able to safely produce amorphous riboflavin, making it possible to determine for the first time the glass transition temperature of this compound: Tg = 144°C.

3.2. Polymorphism of riboflavin

In Figure 2 (red curve), further heating of the milling induced amorphous riboflavin (run 2) reveals two exothermic events. The first one occurs at around 185 °C (ΔH_1 = 58.2 J/g) and is characteristic of a recrystallization. The diffractogram of the milled material subsequently heated to 200°C, recorded at room temperature (i.e. just above the first exotherm), is reported in Figure 1 (black curve). It shows well defined Bragg peaks, characteristic of a crystalline state. Moreover, these peaks are clearly different from those characteristic for Form I (see for instance characteristic peaks marked with a ★ or ◆ in Figure 1). This indicates that the recrystallization occurred at 185°C toward another crystalline form of riboflavin, called “Form III” ([37]). The second exotherm in run 2 (red curve in Figure 2) occurs at around 230 °C (ΔH_2 = 34.1 J/g) and is characteristic of a “crystal to crystal” transformation. The diffractogram of the milled material recorded at room temperature after subsequent heating to 240°C (i.e. just above the second exotherm), is also reported in Figure 1 (green curve). It shows well defined Bragg peaks, which are different from those of Forms I and III (see for instance characteristic pics marked with a ★, ◆ or ▲ in Figure 1). This confirms that the second exotherm indicates a polymorphic transformation, and puts into evidence a further polymorphic form of riboflavin, called “Form II” [37]. Above 240 °C, run 3 shows an endothermic peak due to the melting of Form II, being superimposed with the exothermic peak due to the degradation of riboflavin (red curve in Figure 2). It can be noted that the melting of Form II is depressed compared to the melting of Form I.

The green and black curves in Figure 3 show the ^{1}H NMR spectra of both, Form II and Form III. They appear to be identical with the spectrum of Form I, with an additional peak attributed to residual acetone (as for the milled material, please see above). Furthermore, no sign for vitamin degradation was observed, which indicates that the polymorphic forms of riboflavin can be safely produced by the described milling and subsequent heating procedures.

3.3. Influence of the milling time upon recrystallization

Figure 4 shows XRD patterns of riboflavin recorded after various milling times ranging from “zero” (no milling) to 32 h. A progressive flattening and broadening of the Bragg peaks can be noted. The decrease in peak heights indicates the increasing amorphization of the material, while the broadening signals both: size reduction and the deformation of the remaining crystallites induced by the mechanical impacts of the milling balls. After 6 h milling, the Bragg peaks totally disappeared, indicating that the material was fully amorphized. No further evolution of the X-ray diffraction patterns can be detected for longer milling times (up to 32 h).

The corresponding heating DSC scans (5 °C/min) are illustrated in Figure 5. They show the progressive development of a heat capacity (Cp) jump at the glass transition temperature (Tg = 144°C), followed by a crystallization exotherm. The Cp jump becomes stationary from 6 h milling, which confirms that the amorphization upon milling is complete after that time period. The evolution of the exotherm is more complex: It shows in particular a shift from 160 to 180 °C, which reveals an increasing stability of the amorphous fraction for increasing milling times. Moreover, noticeable modifications of the thermograms are still observed for longer milling times. In particular, a second exotherm develops after the recrystallization. It is already detectable after 3 and 6 h milling through a shouldering on the right-hand side of the recrystallization exotherm and then shifts toward higher temperatures up to 230 °C after 32 h milling. This exothermic peak clearly corresponds to the polymorphic transformation “Form III → Form II” identified in *section 3.2*. This indicates that the structural composition of the recrystallized fraction depends on the milling time. To analyze this point in more detail, the structure of the recrystallized material has been investigated by XRD.

Figure 6 shows XRD patterns of riboflavin recorded at room temperature after milling for 50 min, 6, 12 or 32 h and subsequent heating (5 °C/min) to 210, 176, 195 and 200 °C, respectively (i.e. after recrystallization of the milled materials). It shows that for 50 min milling and heating to 210 °C, the X-ray diffraction patterns of the recrystallized

material only shows the Bragg peaks of Form I, while Bragg peaks characteristic for Forms II and III cannot be detected. This indicates that for short milling times the portion of riboflavin, which has been transformed into an amorphous state (Figure 4) recrystallizes entirely towards the initial Form I. This can be explained by the numerous remaining crystallites of Form I after 50 min milling, which act as seeds for the recrystallization of Form I upon heating. Interestingly, complete amorphization upon milling for milling times > 6 h and subsequent heating leads to the crystallization of different polymorphic forms: as it can be seen in Figure 6, the X-ray diffraction patterns of the samples, which had been milled for 6, 12 or 32 h, followed by heating to 176, 195 and 200 °C, do not show the Bragg peaks of Form I. Instead, they show the Bragg peaks of the Forms II and III. Moreover, with increasing milling time the Bragg peaks characteristic of Form III become more pronounced, while those of Form II decrease and finally disappear after 32 hours of milling. This indicates that riboflavin is fully amorphized upon milling for more than 6 h and recrystallizes as a mixture of Forms II and III, with a proportion of Form III, which increases with increasing milling time. Such a behavior could be due to the apparent stabilization of amorphized riboflavin with increasing milling time, shifting the recrystallization range toward higher temperatures, at which the nucleation and growth rates of Form III are higher than those of Form II.

3.4. Phase diagram of riboflavin

To determine the relative stability of Forms I, II and III, it is necessary to rank their melting temperatures. However, the melting temperatures of Forms I and II cannot be accurately determined due to the strong degradation accompanying the melting process (see runs 1 and 3 in Figure 2). Moreover, the melting of Form III cannot be observed as it is preceded by the conversion “Form III → Form II” (see run 2 Figure 2). To overcome these difficulties, the three forms have been analyzed by flash DSC at a heating rate of 300 °C/s. Such a high heating rate makes it possible to by-pass the transformation “Form III → Form II” in order to observe the melting of Form III, and strongly limit the degradation accompanying the melting process. The corresponding

scans are reported in Figure 7 and do not show any trace of the transformation “Form III → Form II”, nor noticeable degradation. It appears that the melting temperatures of the three forms rank as follows: Tm(I)>Tm(III)>Tm(II). Moreover, the exothermic character of the transformation “Form III → Form II” seen in run 2 in Figure 2 indicates that the entropy of Form III is higher than that of Form II. As a result, these two forms are enantiotropically related as schematized in the Gibbs free enthalpy diagram reported in Figure 8.

3.5. Dissolution kinetics of the different forms of riboflavin

In order to monitor the dissolution kinetics of the different riboflavin forms, sufficient sample quantities were required (about 150 mg). Form I was used as received. The amorphous form was obtained by milling Form I for 32 h in a high energy planetary mill (Pulverisette 7 Fritsch). Samples of Forms III and II were produced as follows: milling of Form I for 32 h in the planetary mill, followed by heating in a DSC Tzero open pan (5 °C/min) to either 200 or 250 °C, respectively. This procedure was repeated several times in order to produce the required amounts (150 mg). The obtained samples were slightly hand milled and the powders pooled.

Figure 9 shows SEM pictures of the different powders used for dissolution testing. Amorphous riboflavin and Form I powders consisted of tiny particles. The amorphous particles formed aggregates, those of Form I were needle-shaped. In contrast, the particles of Form II and Form III were much larger, because they were prepared by manual milling (versus planetary milling). But at higher magnification, also in these cases, tiny needle-shaped crystals could be observed.

The dissolution kinetics of these powders in ultra-pure water at 37 °C under non-sink conditions (excess of solid riboflavin) are illustrated in Figure 10. Clearly, amorphous riboflavin led to the highest concentration of dissolved riboflavin within the first few hours: up to around 1860 mg/L. But at later time points (after 24 h), this concentration decreased to about 330 mg/L, and then leveled-off. In contrast, Form I was much less soluble (around 90 mg/L) and reached its plateau concentration within the first few

hours. Forms II and III reached intermediate concentrations of dissolved riboflavin during the first 4 h: about 450 mg/L. But the latter decreased again, reaching plateau values of approximately 350 and 300 mg/L, respectively, after about 7 d.

The observed vitamin dissolution patterns can be explained as follows: The solubility of the amorphous riboflavin is highest, leading to the highest observed *dissolved* vitamin concentrations. However, at later time points (after at least 4 h), the vitamin recrystallizes into a less soluble form (red curve in Figure 10). Form I exhibits the lowest solubility (which is consistent with the highest melting point observed by flash DSC, Figure 7), leading to the lowest concentrations of dissolved riboflavin. Forms II and III have intermediate solubilities, resulting in intermediate dissolution rates. However, also in these cases a different form precipitates at later time points during the experiment.

To better understand which riboflavin form crystallizes during the dissolution measurements, the solids obtained after 7 d were separated by filtration, dried (under vacuum, room temperature, overnight) and analyzed by XRD and TGA. Figure 11 shows the XRD patterns of the residue obtained at the end of the dissolution study of amorphous riboflavin. Interestingly, it differs from those of Forms I, II and III (see in particular the peak at 4.3 °), but seems to be similar to that of a dihydrate reported in the literature [31]. The TGA scan (5 °C/min) of the residue, which is reported in the insert of Figure 11, shows a mass loss of close to 6.0 % between 20 and 80 °C, while a mass loss of 9.2 % would be expected for the dehydration of a dihydrate. The difference may be attributed to a slight dehydration occurring during the vacuum drying prior to TGA analysis. Moreover, the evolution of the diffractogram of the recrystallized solid upon heating (5 °C/min) to 60 °C – i.e. in the temperature range, in which the water loss was observed – is also reported in Figure 11. It shows the progressive appearance and disappearance of some Bragg peaks, which ultimately leads to a X-ray diffraction patterns characteristic of Form II. All these results, thus, indicate that the

amorphous riboflavin dissolved in water, recrystallized toward a dihydrate form, whose dehydration upon heating led to the metastable anhydrous Form II. Please note that identical behaviors were observed for samples, which recrystallized after the dissolution of Forms II and III. The precipitation of the same dihydrate form upon dissolution of amorphous riboflavin and Forms II and III can explain the similar plateau values observed at late time points for these different forms.

4. Conclusion

Amorphous riboflavin (free base) could be obtained for the first time: via high energy milling of a commercial crystalline form (Form I). This solid state amorphization technique was used to avoid the pronounced degradation of the riboflavin, which occurs during melting (and, thus, prevents obtaining the amorphous form via quench cooling of the melt). The glass transition temperature (Tg = 144°C) and the Cp jump at Tg (ΔCp= 0.68 J/g/°C) could, hence, accurately be determined.

Upon heating, amorphous riboflavin was found to show a rich pattern of physical transformations which enlightens the polymorphism of this vitamin. It shows in particular a recrystallization toward Form III occurring at 185 °C (ΔH_1 = 58.2 J/g), followed by a polymorphic transformation toward Form II occurring at 230°C (ΔH_2 = 34.1 J/g). These two forms appear to be enantiotropically related and the relative stability of the three polymorphs at room temperature appears to rank as follow: I > II > III.

Finally, the dissolution kinetics of the different forms in water were evaluated and revealed the following order in the dissolution rates during the first 4 h: amorphous>Forms III ≈ Form II>Form I. After 4 h, a drop in the amount of dissolved riboflavin occurred for the amorphous and metastable crystalline forms due to a recrystallization toward a dihydrate. However, the plateau values were above the solubility of Form I, revealing definitely the faster dissolution of the metastable forms (II, III and amorphous) over the stable crystalline Form I.

Acknowledgements

This project has received funding from the European Union's Horizon 2020 research and innovation programme under the Marie Sktodowska-Curie grant agreement No 847568.

Declaration of Competing Interest

The Editor-in-Chief of the journal is one of the co-authors of this article. The manuscript has been subject to all of the journal's usual procedures, including peer review, which has been handled independently of the Editor-in-Chief.

CAPTIONS:

Figure 1: X-Ray diffraction patterns of riboflavin Form I recorded at room temperature before and after different mechanical and thermal treatments. From top to bottom: before milling (Form I); after 32 h milling (amorphous form); after 32 h milling and subsequent heating to 200°C (Form III); after 32 h milling and subsequent heating to 240°C (Form II).

Figure 2: TGA scan (5 °C/min) of commercial riboflavin (Form I) and DSC heating scans (5 °C/min) of non-milled (run 1) riboflavin as well as of milled riboflavin (Form I) (runs 2 and 3). The symbol (//) separates run 2 (using a standard open aluminum pan) from run 3 (using a hermetically sealed pan).

Figure 3: ^{1}H NMR spectra of riboflavin Form I non-milled (as received), quenched from the melt, milled for 32 h, as well as of riboflavin Form II and Form III. To better see the small peaks and avoid anarchic superimposition of the different spectra, the highest peaks have been clipped.

Figure 4: XRD patterns of riboflavin Form I recorded after different milling times (t_m) ranging from zero (no milling) to 32 h. The milling times are reported on the right-hand side of each diffraction pattern.

Figure 5: DSC scans (5 °C/min) of riboflavin Form I recorded after different milling times (t_m) ranging from zero (no milling) to 32 h. The milling times are reported on the left-hand side of each thermogram.

Figure 6: XRD patterns recorded at room temperature of riboflavin, which had been milled for 50 min, 6, 12 or 32 h, and subsequently heated (5 °C/min) to 210, 176, 195 or 200°C, respectively.

Figure 7: Flash DSC scans (300 °C/s) of Forms I, II and III of riboflavin.

Figure 8: Phase diagram of riboflavin. The arrows indicate the trajectory of riboflavin during the milling and subsequent heating of Form I.

Figure 9: SEM pictures of the different riboflavin powders used for dissolution measurements.

Figure 10: Dissolution kinetics of the different forms of riboflavin in ultra-pure water at 37°C under agitation (80 rpm) and non-sink conditions: A large excess of non-dissolved vitamin was provided throughout the experiments.

Figure 11: XRD patterns of the solid which reprecipitated during the dissolution study of amorphous riboflavin in water. The samples were heated at 5 °C/min followed by an isothermal of about 13 min (scan duration) at different temperatures (as indicated). Insert: TGA scan (5 °C/min) of the reprecipitated solid (without heating).

Figure 1

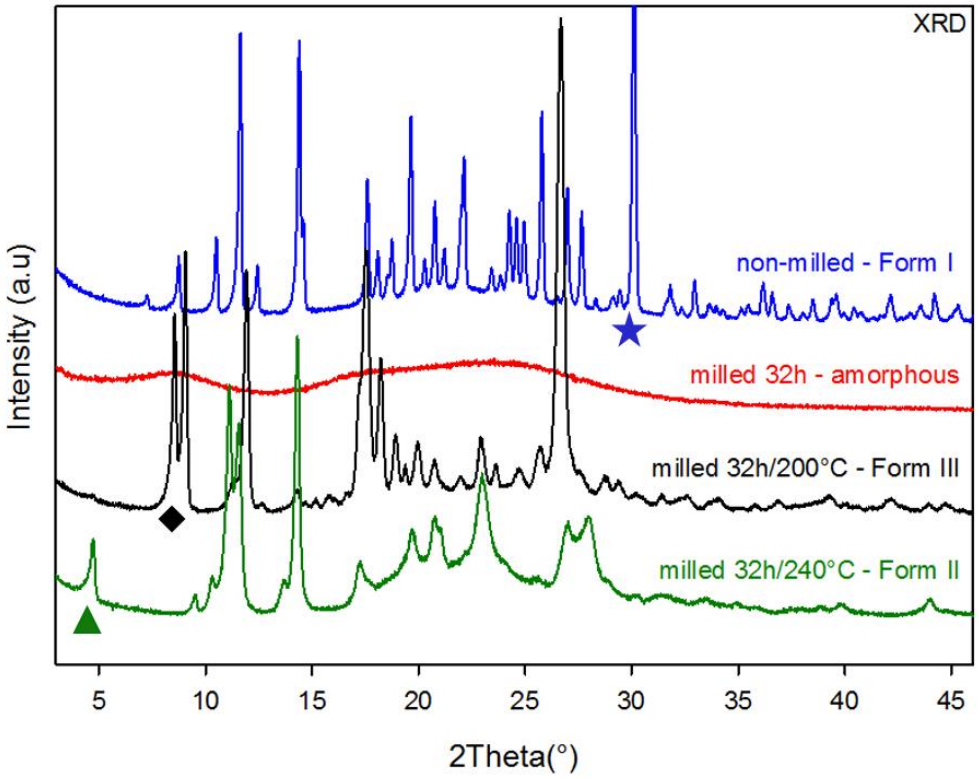
XRD
non-milled - Form I
milled 32h - amorphous
milled 32h/200°C - Form III
milled 32h/240°C - Form II
Intensity (a.u)
5
10
15
20
25
30
35
40
45
2Theta(°)

Figure 2

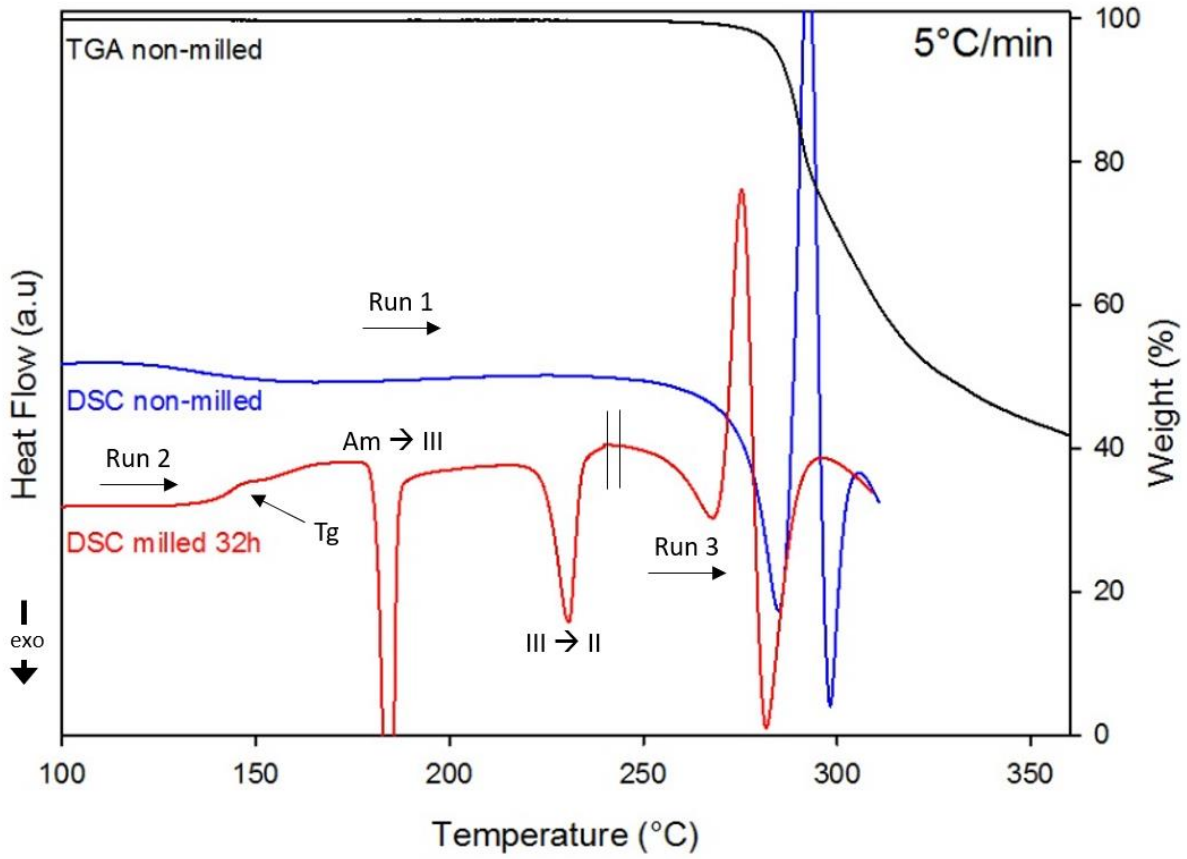
TGA non-milled
5°C/min
Run 1
DSC non-milled
Run 2
Am → III
Tg
DSC milled 32h
III → II
Run 3
exo
Heat Flow (a.u)
Weight (%)
Temperature (°C)
100
150
200
250
300
350
0
20
40
60
80
100

Figure 3

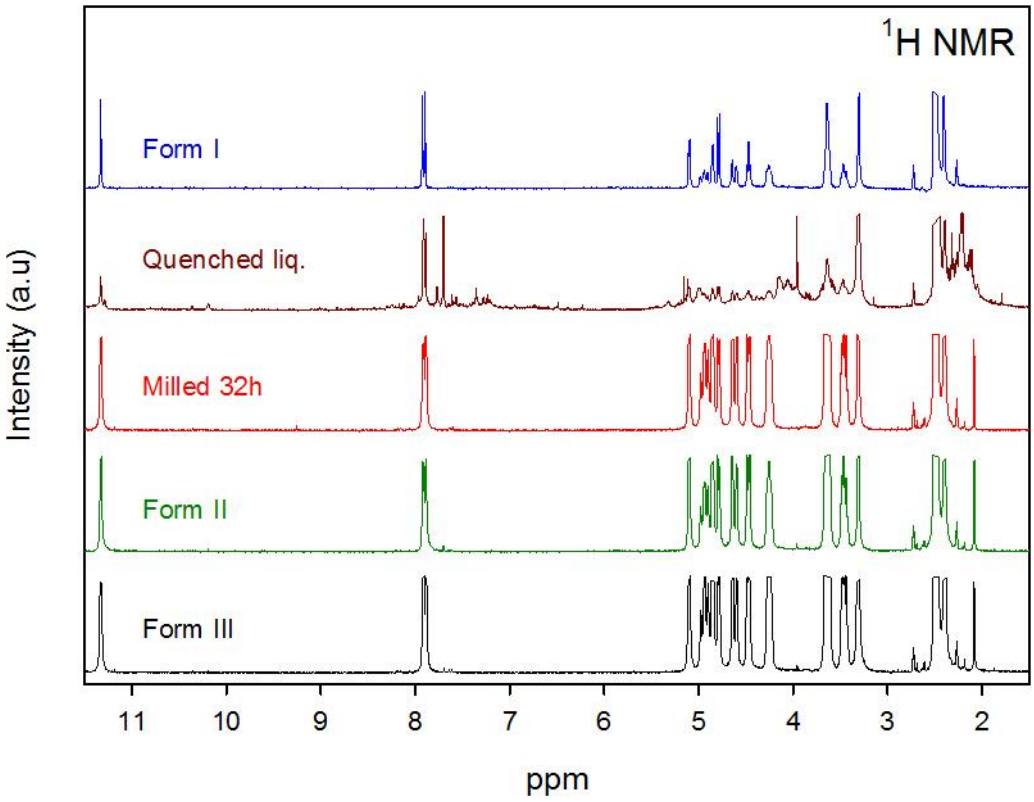
^{1}H NMR
Form I
Quenched liq.
Milled 32h
Form II
Form III
Intensity (a.u)
11
10
9
8
7
6
5
4
3
2
ppm

Figure 4

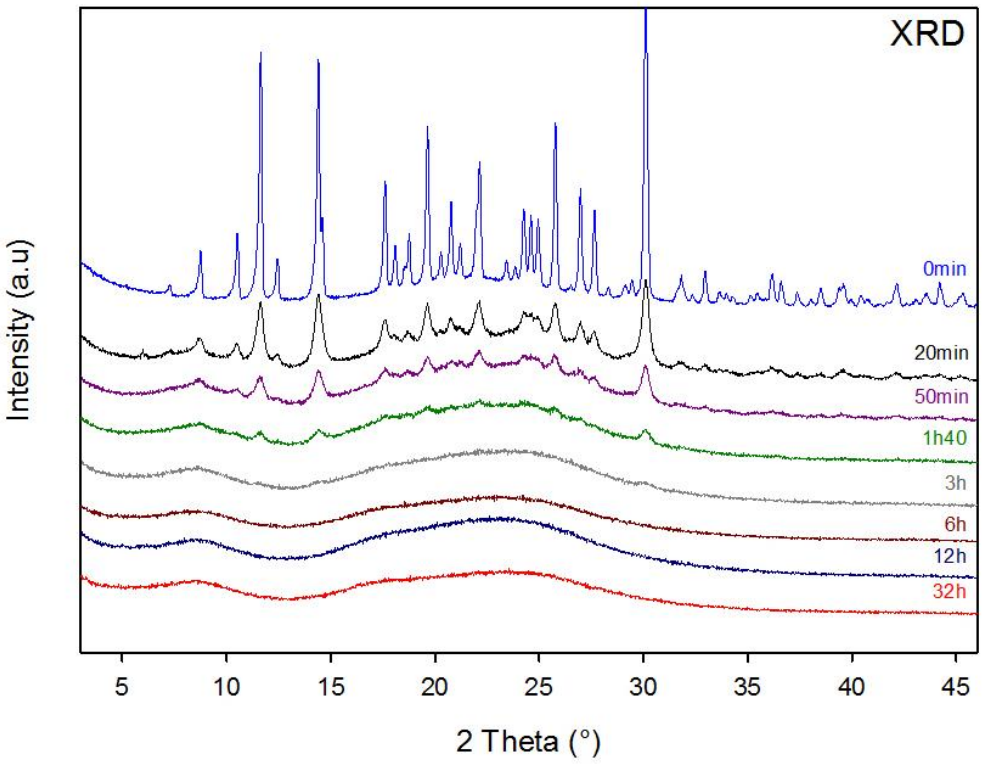

Figure 5

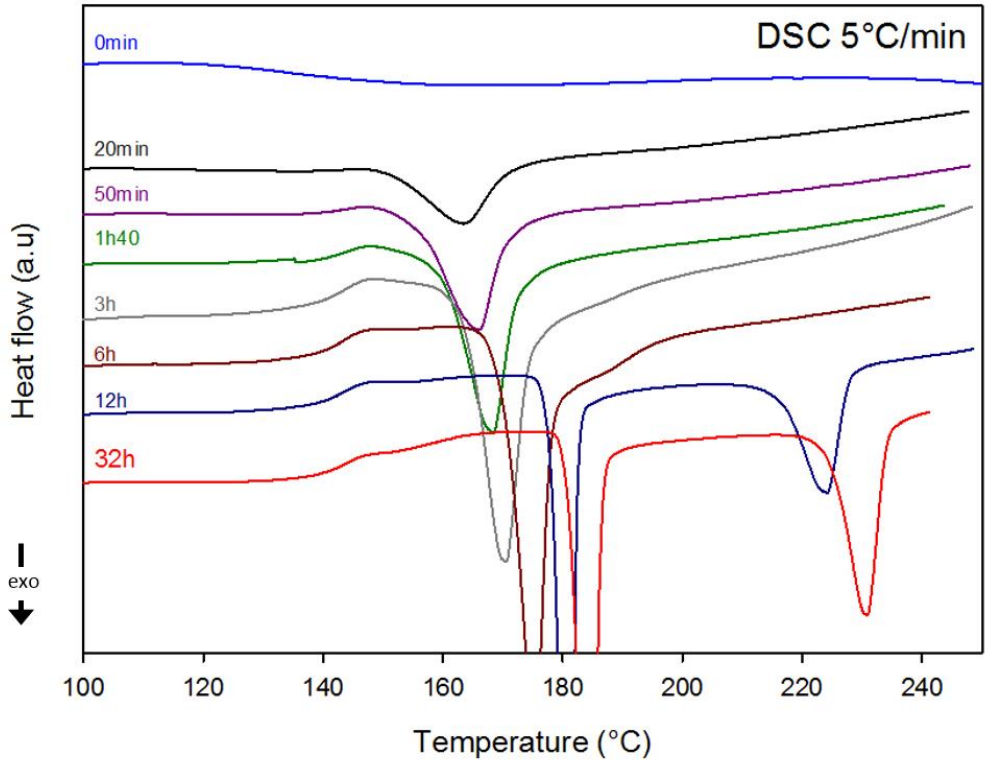

Figure 6

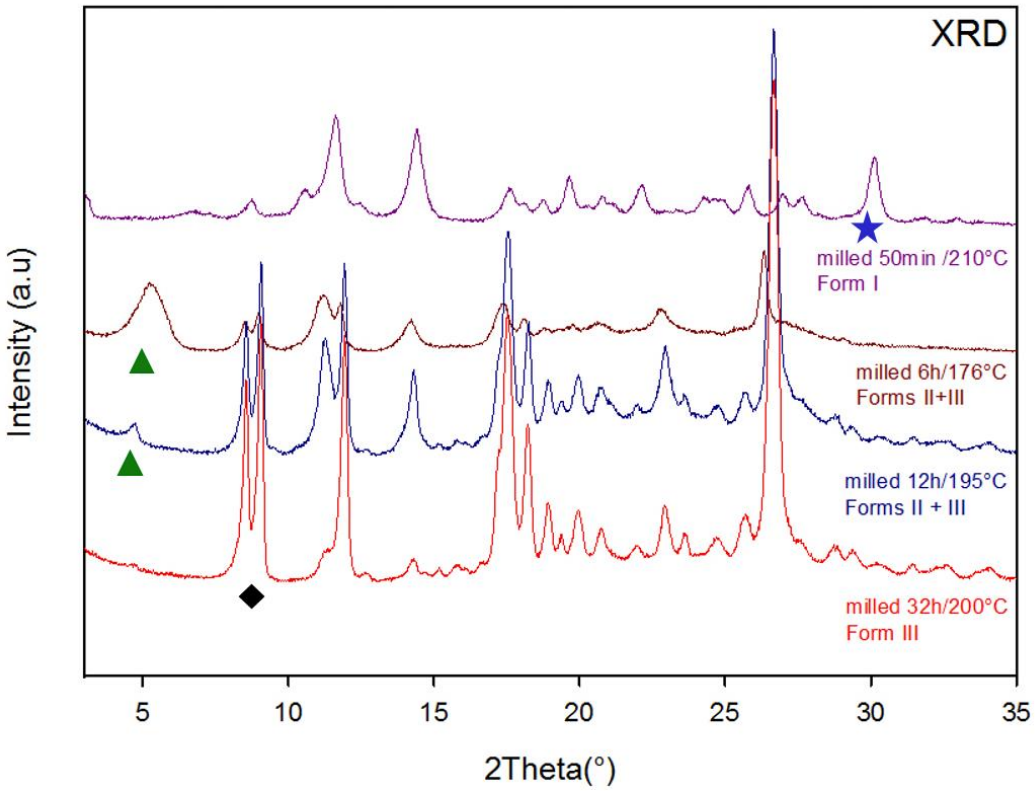
XRD
Intensity (a.u)
2Theta(°)
5
10
15
20
25
30
35
milled 50min /210°C
Form I
milled 6h/176°C
Forms II+III
milled 12h/195°C
Forms II + III
milled 32h/200°C
Form III

Figure 7

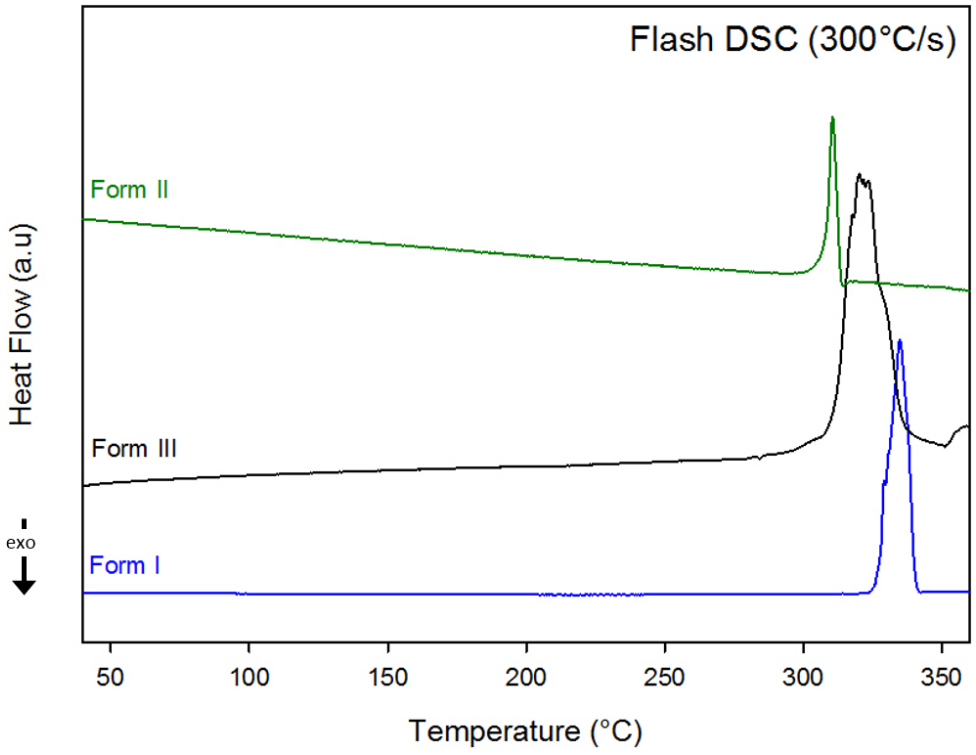

Figure 8

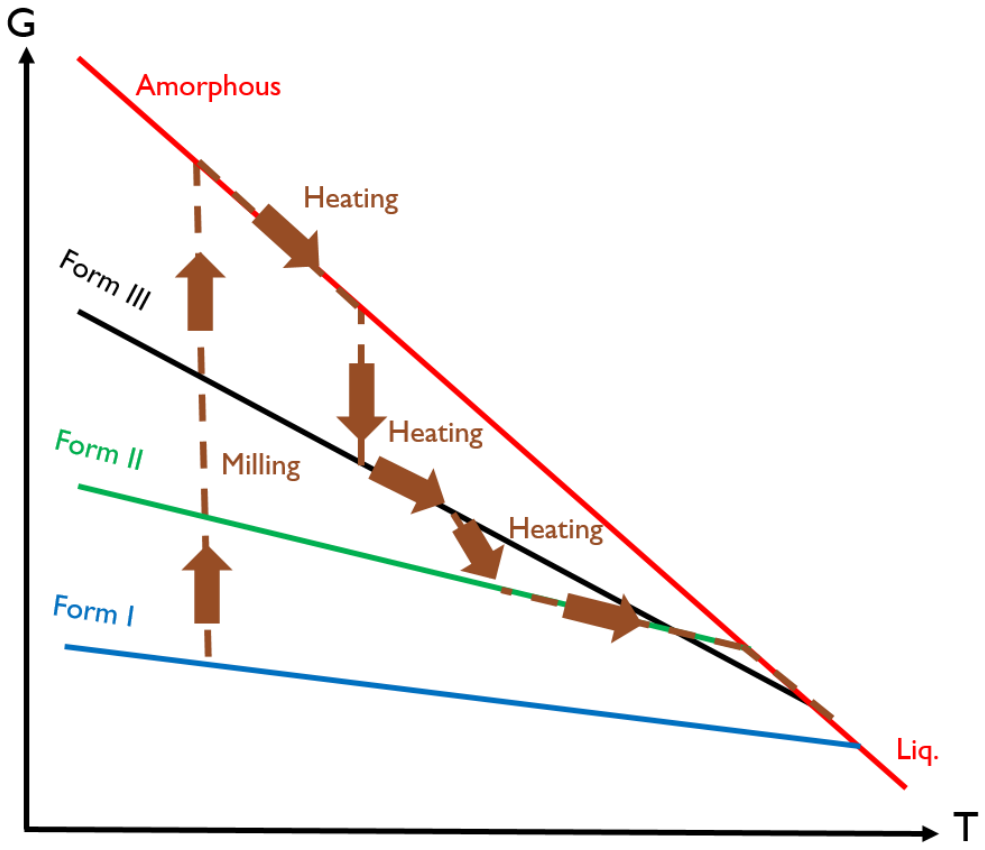

Figure 9

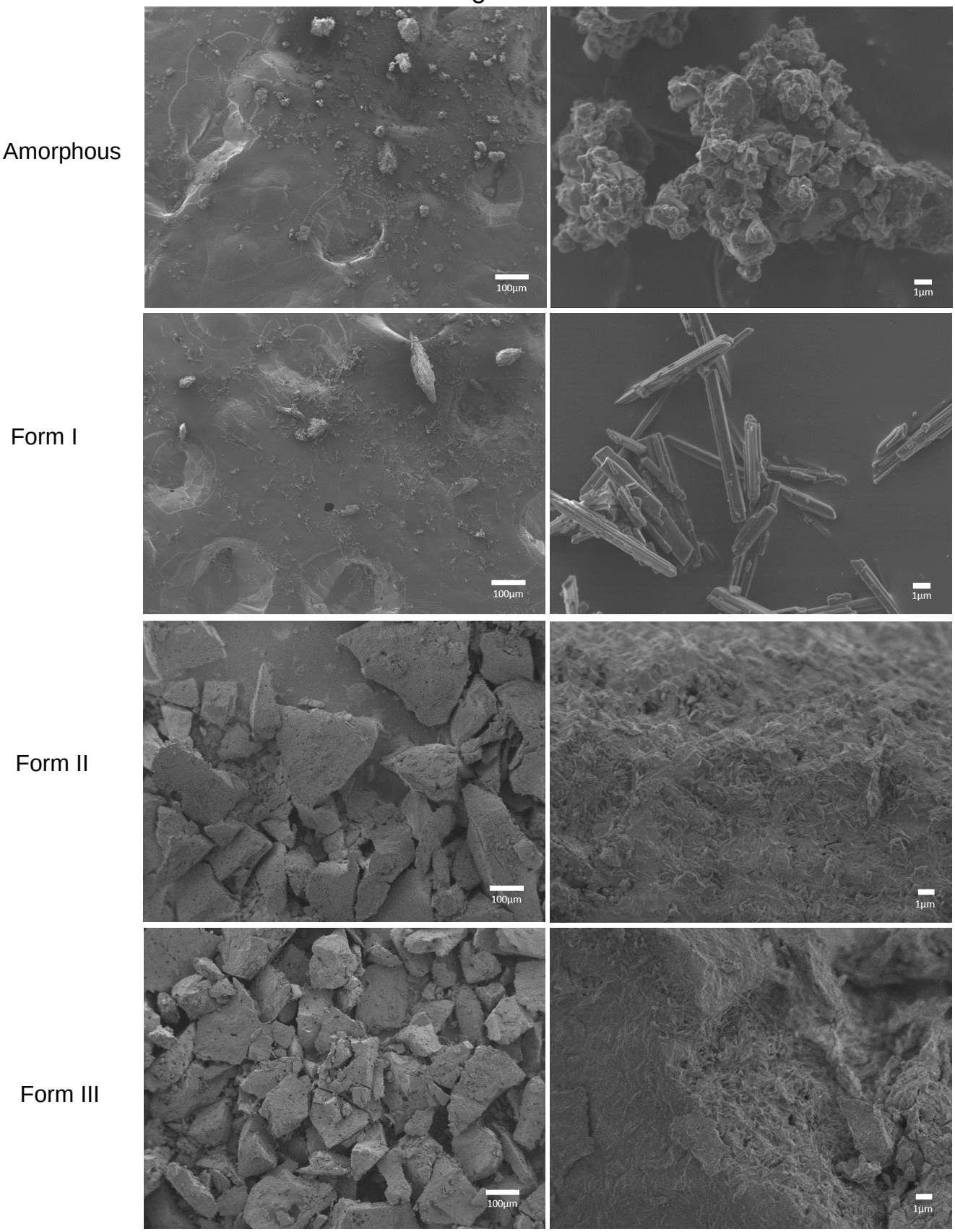

Figure 10

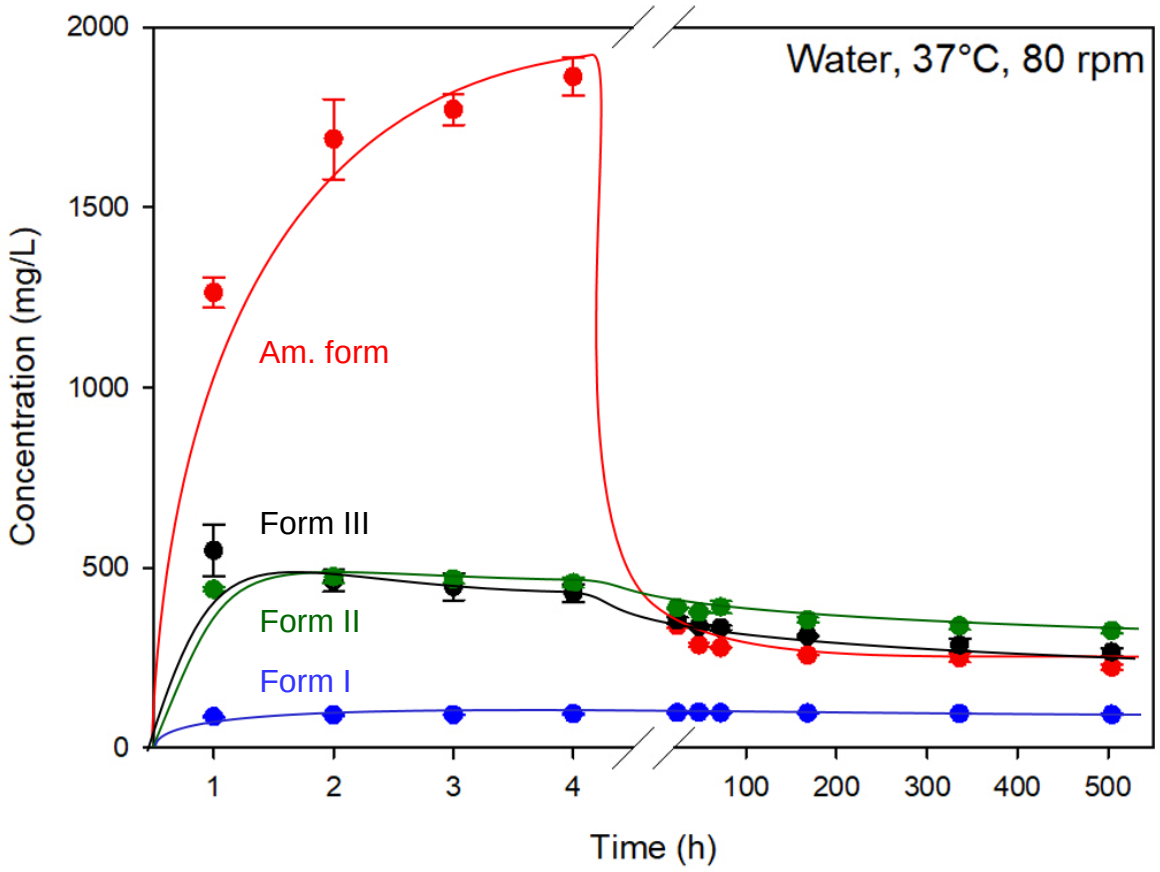
Water, 37°C, 80 rpm
Concentration (mg/L)
Time (h)
Am. form
Form III
Form II
Form I
2000
1500
1000
500
0
1
2
3
4
100
200
300
400
500

Figure 11

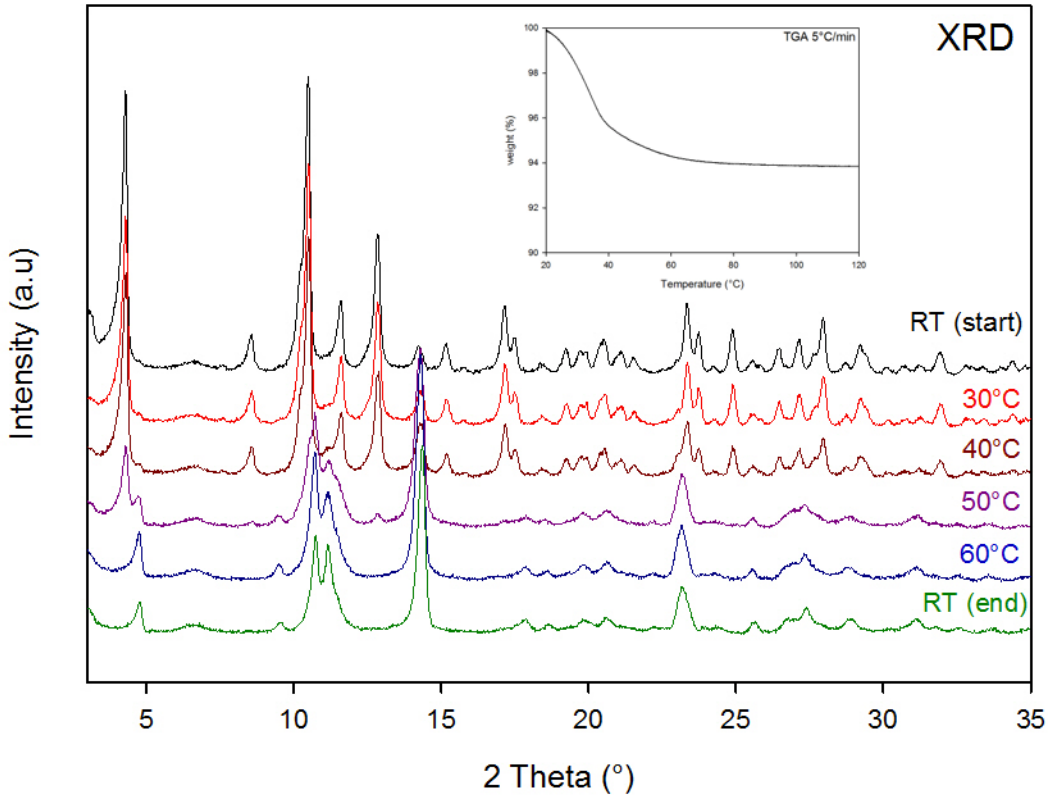
XRD
TGA 5°C/min
weight (%)
Temperature (°C)
RT (start)
30°C
40°C
50°C
60°C
RT (end)
Intensity (a.u)
2 Theta (°)

REFERENCES

[1] H. G. Brittain, *Polymorphism in pharmaceutical solids*. in Drugs and the pharmaceutical sciences. New York: M. Dekker, 1999. Accessed: Mar. 10, 2023. [Online]. Available: https://search.ebscohost.com/login.aspx?direct=true&scope=site&db=nlebk&db=nlabk&AN=12783

[2] R. Hilfiker, F. Blatter, and M. von Raumer, "Relevance of Solid-state Properties for Pharmaceutical Products," in *Polymorphism*, John Wiley & Sons, Ltd, 2006, pp. 1–19. doi: 10.1002/3527607889.ch1.

[3] R. J. Davey, "Polymorphism in Molecular Crystals Joel Bernstein. Oxford University Press, New York, 2002. ISBN 0198506058.," *Cryst. Growth Des.*, vol. 2, no. 6, pp. 675–676, Nov. 2002, doi: 10.1021/cg020039a.

[4] L. Yu, "Polymorphism in Molecular Solids: An Extraordinary System of Red, Orange, and Yellow Crystals," *Acc. Chem. Res.*, vol. 43, no. 9, pp. 1257–1266, Sep. 2010, doi: 10.1021/ar100040r.

[5] B. C. Hancock and G. Zografi, "Characteristics and significance of the amorphous state in pharmaceutical systems," *J. Pharm. Sci.*, vol. 86, no. 1, pp. 1–12, Jan. 1997, doi: 10.1021/js9601896.

[6] M. Descamps, E. Dudognon, and J.-F. Willart, *The amorphous state*. Wiley-VCH, 2019. doi: 10/18033.

[7] Y. Sun, L. Zhu, T. Wu, T. Cai, E. Gunn, and L. Yu, "Stability of Amorphous Pharmaceutical Solids: Crystal Growth Mechanisms and Effect of Polymer Additives," *AAPS J.*, vol. 14, pp. 380–8, Mar. 2012, doi: 10.1208/s12248-012-9345-6.

[8] K. A. Graeser, J. E. Patterson, and T. Rades, "Physical stability of amorphous drugs: Evaluation of thermodynamic and kinetic parameters," in *Journal of Pharmacy and Pharmacology*, PHARMACEUTICAL PRESS-ROYAL PHARMACEUTICAL SOC GREAT BRITIAN 1 LAMBETH HIGH …, 2008, pp. A46–A46.

[9] B. C. Hancock and M. Parks, "What is the true solubility advantage for amorphous pharmaceuticals?," *Pharm. Res.*, vol. 17, no. 4, pp. 397–404, Apr. 2000, doi: 10.1023/a:1007516718048.

[10] S. B. Murdande, M. J. Pikal, R. M. Shanker, and R. H. Bogner, "Solubility advantage of amorphous pharmaceuticals: I. A thermodynamic analysis," *J. Pharm. Sci.*, vol. 99, no. 3, pp. 1254–1264, Mar. 2010, doi: 10.1002/jps.21903.
[11] D. Q. Craig, P. G. Royall, V. L. Kett, and M. L. Hopton, "The relevance of the amorphous state to pharmaceutical dosage forms: glassy drugs and freeze dried systems," *Int. J. Pharm.*, vol. 179, no. 2, pp. 179–207, Mar. 1999, doi: 10.1016/s0378-5173(98)00338-x.
[12] A. Mahieu, J. Willart, E. Dudognon, F. Danède, and M. Descamps, "A New Protocol To Determine the Solubility of Drugs into Polymer Matrixes," *Mol. Pharm.*, vol. 10, Dec. 2012, doi: 10.1021/mp3002254.
[13] M. Davis and G. Walker, "Recent strategies in spray drying for the enhanced bioavailability of poorly water-soluble drugs," *J. Control. Release Off. J. Control. Release Soc.*, vol. 269, pp. 110–127, Jan. 2018, doi: 10.1016/j.jconrel.2017.11.005.
[14] J. E. Patterson, M. B. James, A. H. Forster, R. W. Lancaster, J. M. Butler, and T. Rades, "Preparation of glass solutions of three poorly water soluble drugs by spray drying, melt extrusion and ball milling," *Int. J. Pharm.*, vol. 336, no. 1, pp. 22–34, May 2007, doi: 10.1016/j.ijpharm.2006.11.030.
[15] A. T. Serajuddin, "Solid dispersion of poorly water-soluble drugs: early promises, subsequent problems, and recent breakthroughs," *J. Pharm. Sci.*, vol. 88, no. 10, pp. 1058–1066, Oct. 1999, doi: 10.1021/js980403l.
[16] C. Tizaoui, H. Galai, S. Clevers, N. Couvrat, G. Coquerel, and I. B. Rietveld, "The persistence and crystallization behavior of atorvastatin calcium amorphous dispersions in polyvinylpyrrolidone," *J. Drug Deliv. Sci. Technol.*, vol. 72, p. 103375, Jun. 2022, doi: 10.1016/j.jddst.2022.103375.
[17] M. Bauer *et al.*, "On the dimorphism of prednisolone: The topological pressure-temperature phase diagram involving forms I and II," *Int. J. Pharm.*, vol. 624, p. 122047, Aug. 2022, doi: 10.1016/j.ijpharm.2022.122047.
[18] M. A. Neumann, J. van de Streek, F. P. A. Fabbiani, P. Hidber, and O. Grassmann, "Combined crystal structure prediction and

high-pressure crystallization in rational pharmaceutical polymorph screening," *Nat. Commun.*, vol. 6, no. 1, Art. no. 1, Jul. 2015, doi: 10.1038/ncomms8793.
[19] R. Censi and P. Di Martino, "Polymorph Impact on the Bioavailability and Stability of Poorly Soluble Drugs," *Mol. Basel Switz.*, vol. 20, no. 10, pp. 18759–18776, Oct. 2015, doi: 10.3390/molecules201018759.
[20] A. Kapourani, T. Tzakri, V. Valkanioti, K. N. Kontogiannopoulos, and P. Barmpalexis, "Drug crystal growth in ternary amorphous solid dispersions: Effect of surfactants and polymeric matrix-carriers," *Int. J. Pharm. X*, vol. 3, p. 100086, Dec. 2021, doi: 10.1016/j.ijpx.2021.100086.
[21] J. Thiry *et al.*, "Continuous production of itraconazole-based solid dispersions by hot melt extrusion: Preformulation, optimization and design space determination," *Int. J. Pharm.*, vol. 515, no. 1, pp. 114–124, Dec. 2016, doi: 10.1016/j.ijpharm.2016.10.003.
[22] V. R. Kallakunta *et al.*, "Stable amorphous solid dispersions of fenofibrate using hot melt extrusion technology: Effect of formulation and process parameters for a low glass transition temperature drug," *J. Drug Deliv. Sci. Technol.*, vol. 58, p. 101395, Aug. 2020, doi: 10.1016/j.jddst.2019.101395.
[23] F. Pöstges, K. Kayser, E. Stoyanov, and K. G. Wagner, "Boost of solubility and supersaturation of celecoxib via synergistic interactions of methacrylic acid-ethyl acrylate copolymer (1:1) and hydroxypropyl cellulose in ternary amorphous solid dispersions," *Int. J. Pharm. X*, vol. 4, p. 100115, Dec. 2022, doi: 10.1016/j.ijpx.2022.100115.
[24] A. Ziaee, A. B. Albadarin, L. Padrela, A. Faucher, E. O'Reilly, and G. Walker, "Spray drying ternary amorphous solid dispersions of ibuprofen – An investigation into critical formulation and processing parameters," *Eur. J. Pharm. Biopharm.*, vol. 120, pp. 43–51, Nov. 2017, doi: 10.1016/j.ejpb.2017.08.005.
[25] A. Ousset *et al.*, "Development of a small-scale spray-drying approach for amorphous solid dispersions (ASDs) screening in

early drug development," *Pharm. Dev. Technol.*, vol. 24, pp. 1–47, Oct. 2018, doi: 10.1080/10837450.2018.1534861.
[26] A. Alqurshi, K. L. A. Chan, and P. G. Royall, "In-situ freeze-drying - forming amorphous solids directly within capsules: An investigation of dissolution enhancement for a poorly soluble drug," *Sci. Rep.*, vol. 7, 2017, doi: 10.1038/s41598-017-02676-2.
[27] E. Valkama, O. Haluska, V.-P. Lehto, O. Korhonen, and K. Pajula, "Production and stability of amorphous solid dispersions produced by a Freeze-drying method from DMSO," *Int. J. Pharm.*, vol. 606, p. 120902, Sep. 2021, doi: 10.1016/j.ijpharm.2021.120902.
[28] K. Kondo and T. Rades, "Solventless amorphization and pelletization using a high shear granulator. Part I; feasibility study using indomethacin," *Eur. J. Pharm. Biopharm.*, vol. 181, pp. 147–158, Dec. 2022, doi: 10.1016/j.ejpb.2022.11.010.
[29] J.-F. Willart, M. Durand, L.-E. Briggner, A. Marx, F. Danède, and M. Descamps, "Solid-state amorphization of linaprazan by mechanical milling and evidence of polymorphism," *J. Pharm. Sci.*, vol. 102, no. 7, pp. 2214–2220, Jul. 2013, doi: 10.1002/jps.23573.
[30] J. C. Dinunzio, C. Brough, J. R. Hughey, D. A. Miller, R. O. Williams, and J. W. McGinity, "Fusion production of solid dispersions containing a heat-sensitive active ingredient by hot melt extrusion and Kinetisol dispersing," *Eur. J. Pharm. Biopharm. Off. J. Arbeitsgemeinschaft Pharm. Verfahrenstechnik EV*, vol. 74, no. 2, pp. 340–351, Feb. 2010, doi: 10.1016/j.ejpb.2009.09.007.
[31] N. Le Barc'H, J. M. Grossel, P. Looten, and M. Mathlouthi, "Kinetic study of the mutarotation of D-glucose in concentrated aqueous solution by gas-liquid chromatography," *Food Chem.*, vol. 74, no. 1, pp. 119–124, Jul. 2001, doi: 10.1016/S0308-8146(01)00139-X.
[32] World Health Organization and Food and Agriculture Organization of the United Nations, Eds., *Vitamin and mineral requirements in human nutrition*, 2nd ed. Geneva : Rome: World Health Organization ; FAO, 2004.

[33] S. S. de Farias *et al.*, "Microencapsulation of riboflavin with galactomannan biopolymer and F127: Physico-chemical characterization, antifungal activity and controlled release," *Ind. Crops Prod.*, vol. 118, pp. 271–281, Aug. 2018, doi: 10.1016/j.indcrop.2018.03.039.
[34] A. R. Bourgonje *et al.*, "The effect of riboflavin supplementation on the systemic redox status in healthy volunteers: A post-hoc analysis of the RIBOGUT trial," *Free Radic. Biol. Med.*, vol. 190, pp. 169–178, Sep. 2022, doi: 10.1016/j.freeradbiomed.2022.08.008.
[35] R. E. Coffman and D. O. Kildsig, "Effect of Nicotinamide and Urea on the Solubility of Riboflavin in Various Solvents," *J. Pharm. Sci.*, vol. 85, no. 9, pp. 951–954, Sep. 1996, doi: 10.1021/js960012b.
[36] J. A. Means, T. C. Grenfell, and F. H. Hedger, "Polymorphism of Riboflavin," *J. Am. Pharm. Assoc. Sci. Ed*, vol. 32, no. 2, pp. 51–53, Feb. 1943, doi: 10.1002/jps.3030320205.
[37] A. Gloor, "Process for the purification of riboflavin," US7670800B2, Mar. 02, 2010 Accessed: May 22, 2023. [Online]. Available: https://patents.google.com/patent/US7670800B2/en
[38] M. Guerain *et al.*, "Structure determination of riboflavin by synchrotron high-resolution powder X-ray diffraction," *Acta Crystallogr. Sect. C*, vol. 77, no. 12, pp. 800–806, 2021, doi: 10.1107/S2053229621012171.
[39] J. Koziol, "Studies on Flavins in Organic Solvents-I*. Spectral Characteristics of Riboflavin, Riboflavin Tetrabutyrate and Lumichrome," *Photochem. Photobiol.*, vol. 5, no. 1, pp. 41–54, 1966, doi: 10.1111/j.1751-1097.1966.tb05759.x.
[40] A. Dupont, M. Guerain, F. Danède, and J. F. Willart, "Evidence of transient amorphization during the polymorphic transformation of sorbitol induced by milling," *Int. J. Pharm.*, vol. 623, p. 121929, Jul. 2022, doi: 10.1016/j.ijpharm.2022.121929.
[41] L. T. Ferreira, R. T. Alarcon, G. L. Perpétuo, and G. Bannach, "Investigation and characterization by TG/DTG–DTA and DSC of the fusion of Riboflavin, and its interaction with the

antibiotic norfloxacin in the screening of cocrystal," *J. Therm. Anal. Calorim.*, vol. 136, no. 2, pp. 581–588, Apr. 2019, doi: 10.1007/s10973-018-7696-7.
[42] E. Elisei, J.-F. Willart, F. Danède, J. Siepmann, F. Siepmann, and M. Descamps, "Crystalline Polymorphism Emerging From a Milling-Induced Amorphous Form: The Case of Chlorhexidine Dihydrochloride," *J. Pharm. Sci.*, vol. 107, no. 1, pp. 121–126, Jan. 2018, doi: 10.1016/j.xphs.2017.07.003.
[43] N. R. Babij *et al.*, "NMR Chemical Shifts of Trace Impurities: Industrially Preferred Solvents Used in Process and Green Chemistry," *Org. Process Res. Dev.*, vol. 20, no. 3, pp. 661–667, Mar. 2016, doi: 10.1021/acs.oprd.5b00417.